

# ***Ab initio* density-functional study of the equilibrium geometries and the electronic properties of $\text{Li}_{10-n}\text{Sn}_n$ ( $n=0-10$ ) clusters**

Mal-Soon Lee\* and D. G. Kanhere†

*Centre for Modeling and Simulation, Department of Physics, University of Pune, Ganeshkhind, Pune 411 007, India*

Kavita Joshi‡

*Département de Recherche Fondamentale sur la Matière Condensée, CEA-Grenoble/DSM 17 rue des Martyrs, F-38054 Grenoble Cedex 9, France*

(Received 30 November 2004; revised manuscript received 4 May 2005; published 25 July 2005)

We have employed *ab initio* molecular dynamics to investigate the equilibrium geometries, energetics, and the nature of bonding in mixed Li-Sn clusters. Our studies reveal that a small percentage of Sn in Li-rich clusters introduces significant changes in the equilibrium geometries. It is also seen that the geometries of Sn-rich clusters are influenced by the  $\text{Sn}_{10}$  motif. Analysis of the nature of bonding shows that there are two competing interactions in the clusters: the polar bond between Li-Sn in the mixed clusters and Sn-Sn interaction leading to covalent bond in Sn-rich clusters.

DOI: [10.1103/PhysRevA.72.015201](https://doi.org/10.1103/PhysRevA.72.015201)

PACS number(s): 36.40.Cg, 61.46.+w, 31.15.Ar

In this Brief Report, we present the equilibrium geometries, energetics, and the nature of bonding in a series of Li-Sn clusters;  $\text{Li}_{10-n}\text{Sn}_n$  ( $n=0-10$ ). The present work is motivated by our earlier investigations on single impurity  $\text{Li}_n\text{Sn}$  clusters [1]. It was observed that the impurity (Sn) having higher electronegativity induces a significant charge transfer from Li to Sn, which was shown to affect the finite-temperature properties of  $\text{Li}_6\text{Sn}$  quite significantly [2]. However, the scope of the previous studies was limited to a single impurity case. In the present work, we investigate the series of clusters with varying concentration of the Li and Sn atoms. The interest in Li-Sn mixed system also stems from earlier reports on alkali-metal-group-IV alloys [3]. These alloys show anomalous behavior in properties like electrical resistivity, density of states, and conductivity as a function of concentration of the constituents. Among these systems, Li-group-IV alloys are peculiar. For instance, a peak in the electrical resistivity is observed at 20% Sn concentration for Li-Sn alloy, as compared to 50% for other alkali-metal-Sn alloys. It has been argued that this rather peculiar behavior is due to the completion of octet at 20% Sn concentration in Li-Sn alloys, which results in a pseudogap in the density of states near the Fermi level. Genser *et al.* investigated the nature of bonding in the crystalline as well as the liquid phase of Li-Sn alloy systems [4]. They observed a strong Sn-Sn covalent bond in equiatomic composition, whereas the octet composition showed dominant Li-Sn ionic bond. Wang *et al.* have studied the stability of  $\text{Sn}_4$  tetrahedron in an alkali-metal environment on a series of  $A_n\text{Sn}_4$  ( $A=\text{Li, Na, and K; } n=4-10$ ) clusters using the *ab initio* density-functional method [5]. They found that the Sn tetrahedron is more unstable in Li clusters compared to other alkali-metal clusters. This can be used as a hint for anomalous behavior

seen at 20% Sn concentration in Li-Sn alloys which is absent in other alkali-metal-Sn alloys.

We first note that the ionic radii of Sn (0.71 Å) and Li (0.68 Å) are nearly equal [6], while their electronegativities are 1.7 and 1.0, respectively [7]. Thus a significant charge transfer from Li to Sn is expected. The diatomic binding energies per atom and bond lengths are 0.72 eV and 2.72 Å for Li-Li, 1.00 eV and 2.76 Å for Li-Sn, 1.77 eV and 2.76 Å for Sn-Sn. Interestingly, in spite of considerable variation in the diatomic binding energies, their bond lengths are similar. In this context, it is quite interesting to study the Li-Sn clusters, especially their bonding properties. In this paper, we present the evolutionary trends in equilibrium geometries, bonding, and other properties as a function of Sn content in the clusters.

We employ Born-Oppenheimer molecular dynamics [8] based on the Kohn-Sham (KS) formulation [9] of the density-functional theory to obtain the equilibrium structures. We also use the ultrasoft pseudopotentials [10] and the generalized gradient approximation (GGA), as implemented in the VASP package [11]. For GGA, Perdew-Wang potential [12] is used. For Li-rich clusters, we optimize structures starting from many selected geometries from high-temperature molecular-dynamic runs. Several additional structures are obtained by interchanging the positions of Li and Sn atoms in previously obtained geometries. All structures are considered to be converged when the force on each ion is less than 0.005 eV/Å with a convergence in the total energy of the order of  $10^{-5}$  eV. We investigate the nature of the bonding via electron localization function (ELF) [13] along with the total charge density and the molecular orbitals (MO's) and the details can be found in our previous publications [1].

The ground-state geometries along with some high-energy structures of all the clusters are shown in Figs. 1 and 2. The ground-state geometry of  $\text{Li}_{10}$  consists of two interconnected pentagonal rings [Fig. 1a(i)] with planes perpendicular to each other. The structure with a trapped atom [Fig. 1a(ii)] is

\*Electronic address: mslee@unipune.ernet.in

†Electronic address: kanhere@unipune.ernet.in

‡Electronic address: joshi@drfmc.ceng.cea.fr

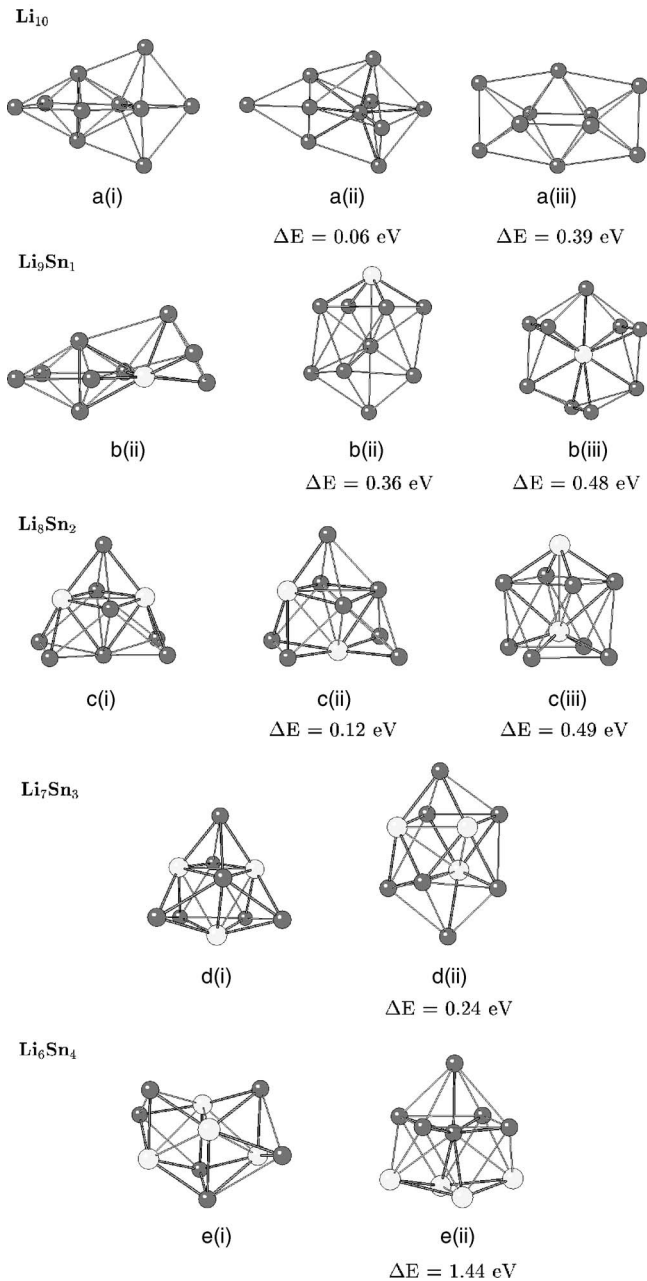


FIG. 1. The equilibrium geometries of the  $\text{Li}_{10-n}\text{Sn}_n$  ( $n=0-4$ ) clusters. The dark circle represents the Li atoms.  $\Delta E$  represents the energy difference with respect to the ground-state energy.

nearly degenerate to the ground-state structure [Fig. 1a(i)]. This structure is found to have the lowest energy within local-density approximation (LDA) by Jones *et al.* [14]. It can be seen that substitution of one Li atom by an Sn atom changes the geometry of the host cluster significantly. The ground-state geometry of  $\text{Li}_9\text{Sn}_1$  [Fig. 1b(i)] consists of only one pentagonal ring, while the other ring, present in  $\text{Li}_{10}$ , is distorted due to the presence of the Sn atom. Other geometries, with the Sn atom as a cap [Fig. 1b(ii)] or at the center [Fig. 1b(iii)], are much higher in energies. This observation is consistent with the fact noted earlier that the most preferred coordination of Sn with Li is 6 and the Sn atom prefers to be on the surface [1]. The ground-state geometry of

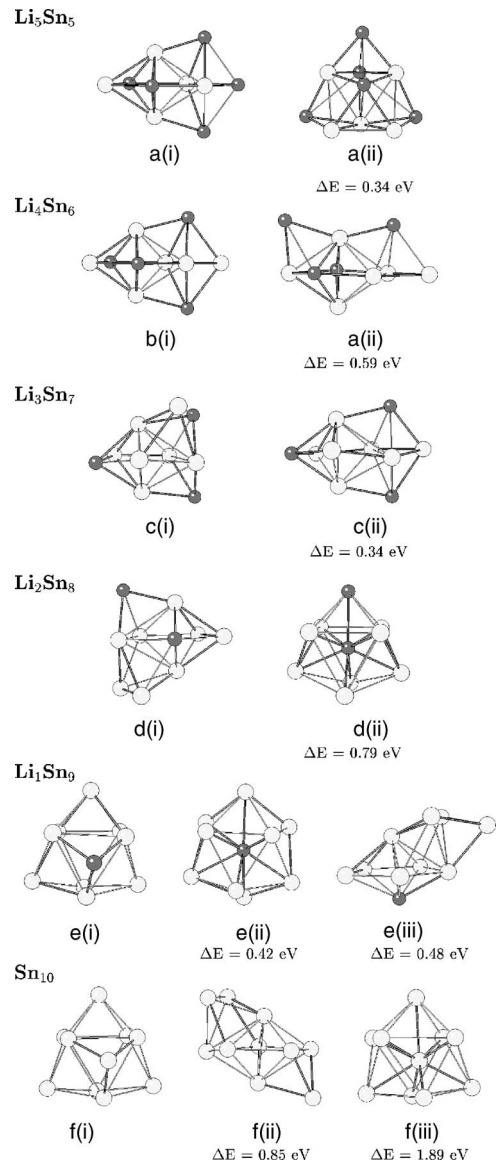


FIG. 2. The equilibrium geometries of the  $\text{Li}_{10-n}\text{Sn}_n$  ( $n=5-10$ ) clusters. The dark circle represents the Li atoms.  $\Delta E$  represents the energy difference with respect to the ground-state energy.

$\text{Li}_8\text{Sn}_2$  [Fig. 1c(i)] shows a symmetric configuration with two Sn atoms separated by a plane of four Li atoms and remaining Li atoms are symmetrically capping both Sn atoms. Evidently, the introduction of a second Sn atom changes the structure significantly making it more compact. Any rearrangement of atoms leads to an unequal distribution of Li atoms with respect to Sn, thereby resulting in high-energy structures [see Figs. 1c(ii) and 1c(iii)]. The ground-state geometry of  $\text{Li}_7\text{Sn}_3$  [Fig. 1d(i)] is very similar to that of  $\text{Li}_8\text{Sn}_2$  [Fig. 1c(i)], except that the additional Sn atom modifies the distribution of the nearby Li atoms so as to optimize the Li-Sn coordination. Replacing one more Li by Sn changes the ground-state geometry drastically as seen in  $\text{Li}_6\text{Sn}_4$  [Fig. 1e(i)] where  $\text{Sn}_4$  forms a bent rhombus structure with Li atoms capping the faces, in agreement with the observation by Wang *et al.* [5]. Such arrangement of Li and Sn atoms optimizes the Li-Sn coordination and minimizes the electro-

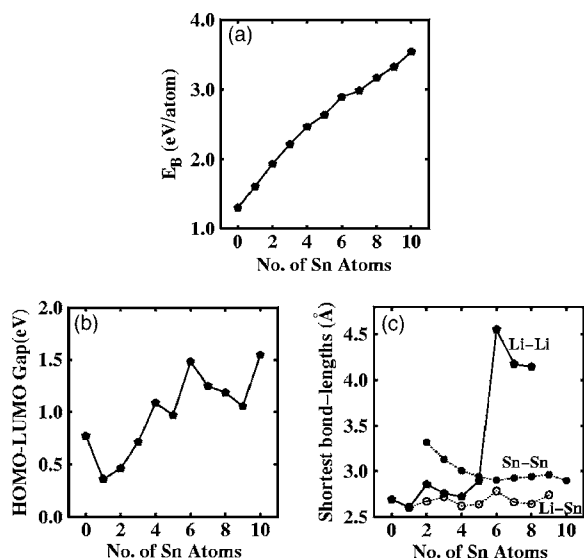


FIG. 3. (a) The binding energy  $E_B$ ; (b) the HOMO-LUMO gap; (c) the shortest bond lengths as a function of number of Sn atoms.

static repulsion. The ground-state geometries of  $\text{Li}_5\text{Sn}_5$  [Fig. 2a(i)] and  $\text{Li}_4\text{Sn}_6$  [Fig. 2b(i)] are similar, consisting of two interconnected pentagonal rings. The lowest energy geometries of  $\text{Li}_3\text{Sn}_7$  [Fig. 2c(i)] and  $\text{Li}_2\text{Sn}_8$  [Fig. 2d(i)] resemble one of the isomers of  $\text{Sn}_{10}$ , shown in Fig. 2f(ii), with some Sn atoms replaced by Li. This geometry can be described as a capped pentagonal bipyramid. The lowest energy structure of  $\text{Li}_1\text{Sn}_9$  [Fig. 2e(i)] is similar to the ground-state geometry of  $\text{Sn}_{10}$  [Fig. 2f(i)] with the tricoordinated Sn atom replaced by an Li atom. The ground-state geometry of  $\text{Sn}_{10}$  [Fig. 2f(i)] is a tetracapped trigonal prism, which has already been reported in the literature [15,16].

We show the binding energy  $E_B$ , the energy gap between the highest occupied molecular orbital (HOMO) and the lowest unoccupied molecular orbital (LUMO), and the shortest bond lengths between Li-Li, Li-Sn, and Sn-Sn in Figs. 3(a)–3(c), respectively. As expected,  $E_B$  increases with increasing Sn content in the cluster [Fig. 3(a)]. The HOMO-LUMO gap [Fig. 3(b)] also increases with the Sn content. It is interesting to see the maximum for clusters with number of electrons 20, 28, and 40 similar to that observed in jellium clusters. It is instructive to examine the change of the nearest-neighbor distances as a function of  $n$ , which is shown in Fig. 3(c). There is hardly any variation in Li-Sn distance, while Sn-Sn distance decreases continuously. While going from  $n=5$  to  $n=6$ , the Li-Li nearest-neighbor distance suddenly jumps to 4.5 Å, indicating that the formation of Sn-Sn bonds becomes more favorable keeping positively charged Li ions far apart. The effect of competing interactions is thus clearly seen in geometries and the relative change in the binding energies.

It may be noted that  $\text{Li}_{10}$  is known to have delocalized charge distribution and Sn to be covalently bonded. A significant charge transfer from Li to Sn leaves Li ions positively charged which in turn polarizes orbitals centered on Sn. Earlier discussion indicates that the cluster tries to minimize energy by balancing two competing interactions, the ionic one between Sn and Li, and the Sn-Sn interaction lead-

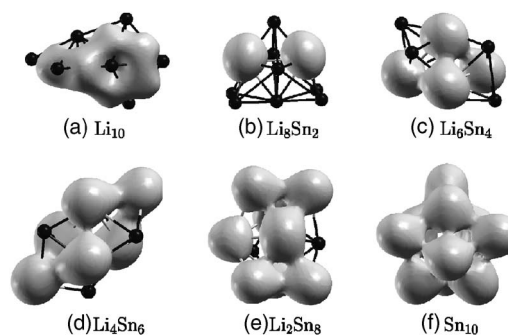


FIG. 4. The isovalued surfaces of the total charge density at 2/3 of its maximum value for the series. The black circles represent Li atoms.

ing to the covalent bond. The mixed clusters studied in the present work also display this complex nature of bonding.

We have investigated the nature of bonding by examining the total charge density, the electron localization function (ELF), and the molecular orbitals (MO's). The isosurfaces of total charge density at 2/3 value of the maximum are shown in Figs. 4(a)–4(f) for  $\text{Li}_{10}$  to  $\text{Sn}_{10}$  for some representative clusters across the series. The dramatic change in the charge density upon introduction of two Sn atoms in  $\text{Li}_{10}$  is evident from Figs. 4(a) and 4(b). The isosurface of  $\text{Li}_{10}$  [Fig. 4(a)] is well spread over the cluster as expected from the jellium model. However, for  $\text{Li}_8\text{Sn}_2$  [Fig. 4(b)] the density is well localized around Sn atoms. A considerable overlap can be seen at 1/3 of the maximum value (figure not shown), which is due to two Sn centered charge densities distorted by the presence of Li ions. The evolution of the localized charge along the Sn-Sn bond can be discerned from Fig. 4. With the increase in Sn content there is an evident increase in the overlap between the nearest-neighbor Sn atoms and the number of such bonds. For example, for four Sn atoms, the overlap is seen only with one of the Sn atoms forming three bonds. The six Sn atoms in  $\text{Li}_4\text{Sn}_6$  [Fig. 4(d)] form two groups, consisting of three atoms each, which form stronger bonds. As the Sn content increases the number of Sn-Sn bonds increases, and finally all Sn atoms are bonded with at least three other Sn atoms in  $\text{Sn}_{10}$ . The picture is consistent with the evolution of nearest-neighbor distance.

The analysis via ELF provides a complimentary approach to charge-density analysis. Let us note that ELF is normalized between 0 and 1. The ELF is large in the region in which Pauli repulsion is small. The higher values of ELF indicate more electron localization in those regions. The spacial points at which the maxima of ELF are located are called attractors and the set of all points connected to this by maximum gradient paths form the basin for that attractor. As the ELF value decreases, the basins merge in to each other. These values are called bifurcation values. It is convenient to discuss the evolution in the nature of bonding via a topological analysis of ELF [13,17]. By examining ELF plots for all the systems, we find that there are as many basins (and attractors) as the number of Sn atoms in the cluster. As the ELF value is decreased these basins merge into each other and the number of such bifurcation points could be larger than 1. The value at which a merger takes place indicates the

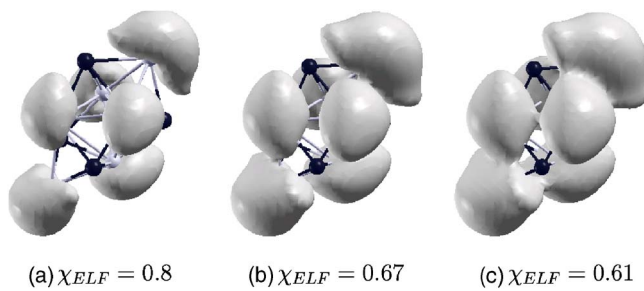


FIG. 5. (Color online) The isovalued surfaces of the electron localization function (ELF) for  $\text{Li}_4\text{Sn}_6$  cluster at different values.

strength and the nature of the bond(s). For example, in the case of  $\text{Li}_8\text{Sn}_2$ , two separate basins around each Sn atom merge at a low value of 0.61, indicating that there is no significant localization in the region between Sn atoms. The value for the first merger increases with Sn content and reaches 0.71 for  $\text{Sn}_{10}$ , again indicating progressive evolution in the nature of bonding between Sn atoms towards covalent bond formation. In Figs. 5(a)–5(c), we show typical ELF isosurfaces with values of 0.8, 0.67, and 0.61 for  $\text{Li}_4\text{Sn}_6$  which depict some of the characteristics noted above. The six basins seen in Fig. 5(a) merge to become two at 0.67 [shown in Fig. 5(b)] and finally merge in to a single one at 0.61 [shown in Fig. 5(c)]. Thus four bonds formed among the three atoms in each basin are stronger than the rest.

It is instructive to examine the molecular orbitals to bring out additional features of bonding. In Fig. 6(a), we show the isodensity surface of typical MO's for the cluster  $\text{Li}_8\text{Sn}_2$ . Figure 6(b) shows the corresponding MO for a  $\text{Sn}_2$  dimer placed at the same distance as in the cluster. In case of pure dimer, the  $\pi$  bonds formed by  $p_z$  orbitals are clearly seen. The significant polarization effect induced by the presence of positively charged Li ions is evident. The bonds are bent toward Li ions and overlapped in the region near Li. A simi-

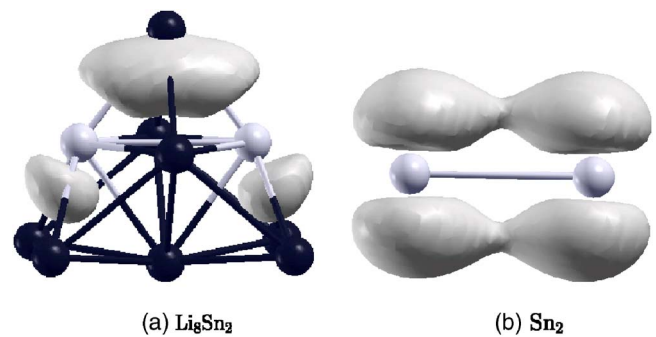


FIG. 6. (Color online) The isodensity surface of a typical MO seen in (a) the third molecular orbital of  $\text{Li}_8\text{Sn}_2$  at 1/2 of its maximum; (b) the fifth molecular orbital of  $\text{Sn}_2$  at 1/4 of its maximum. The black circles represent Li atoms. The bond length of  $\text{Sn}_2$  is the same as that of Sn-Sn bond length in  $\text{Li}_8\text{Sn}_2$ .

lar MO exists for the lower Li ions. It turns out that all the MO's in the clusters studied, except  $\text{Li}_0\text{Sn}_1$ , are Sn-centric and can be traced to the MO's seen in the model system formed by placing Sn atoms in the same geometry as in the Li-Sn clusters.

We have presented the equilibrium geometries, energetics, and the nature of bonding for  $\text{Li}_{10-n}\text{Sn}_n$  ( $n=0-10$ ) clusters obtained by *ab initio* density-functional studies. We find that the geometries of Li-rich clusters change significantly by few Sn impurities. The geometries are governed by a competition between the charge-transfer-induced polar ionic bond between Li and Sn and tendency to form a covalent bond between Sn atoms. The system prefers to minimize energy by formation of Li-Sn bonds whenever possible.

It is a pleasure to acknowledge S. Chacko, S. Shetty, and S. Krishnamurty for useful discussions. We also acknowledge the support of the Indo-French center for promotion of Advance Research.

- 
- [1] Sharan Shetty, Sourav Pal, and Dilip Kanhere, *J. Chem. Phys.* **118**, 7288 (2003); Kavita Joshi and D. G. Kanhere, *Phys. Rev. A* **65**, 043203 (2002).
- [2] Kavita Joshi and D. G. Kanhere, *J. Chem. Phys.* **119**, 12301 (2003).
- [3] T. B. Massalski, H. Okamoto, P. R. Subramanian, and L. Kacprzak, *Binary Alloy Phase Diagrams* (ASM International, Material Parks, Ohio, 1990); W. van der Lugt, *J. Phys.: Condens. Matter* **8**, 6115 (1996).
- [4] O. Genser and J. Hafner, *J. Phys.: Condens. Matter* **13**, 959 (2001); *Phys. Rev. B* **63**, 144204 (2001).
- [5] Bing Wang, M. J. Stott, and J. A. Alonso, *Phys. Rev. B* **65**, 045410 (2002).
- [6] C. Kittel, *Introduction to Solid State Physics* (Wiley, New York, 1986).
- [7] L. Pauling, *Nature of Chemical Bond* (Oxford and IBH, New Delhi, 1967).
- [8] M. C. Payne, M. P. Teter, D. C. Allan, T. A. Arias, and J. D. Joannopoulos, *Rev. Mod. Phys.* **64**, 1045 (1992).
- [9] W. Kohn and L. J. Sham, *Phys. Rev.* **140**, A1133 (1965).
- [10] D. Vanderbilt, *Phys. Rev. B* **41**, R7892 (1990).
- [11] *Vienna Ab initio Simulation Package* (VASP), Technische Universität Wien, 1999.
- [12] J. P. Perdew and Y. Wang, *Phys. Rev. B* **45**, 13244 (1992).
- [13] B. Silvi and A. Savin, *Nature (London)* **371**, 683 (1994).
- [14] R. O. Jones, A. I. Lichtenstein, and J. Hutter, *J. Chem. Phys.* **106**, 4566 (1996).
- [15] Bing Wang, L. M. Molina, M. J. López, A. Rubio, J. A. Alonso, and M. J. Stott, *Ann. Phys.* **7**, 107 (1998).
- [16] Kavita Joshi, D. G. Kanhere, and S. A. Blundell, *Phys. Rev. B* **66**, 155329 (2002).
- [17] Roger Rousseau and Dominik Marx, *Chem.-Eur. J.* **6**, 2982 (2000); A. Savin, R. Nesper, S. Wengert, and T. F. Fässler, *Angew. Chem.* **109**, 1892 (1997); *Angew. Chem., Int. Ed. Engl.* **36**, 1808 (1997).